Microsyst Technol (2017) 23:1485–1494
DOI 10.1007/s00542-016-3254-z

TECHNICAL PAPER

Dynamic analysis of a recirculation system of micro functional fluids for ink-jet applications

Ivan Arango[1] · **Manuel Cañas**[1]

Received: 19 September 2016 / Accepted: 20 December 2016 / Published online: 18 January 2017

Abstract The rise of ink-jet printing technology has led to numerous studies about functional fluids, which, in most cases, are made to change and improve the chemical and rheological properties. Besides this, there are several patents about the recirculation fluid system that help to prevent settling particles, and thus improving print quality without consequences in the chemical composition of the fluid. This paper presents a dynamic analysis of a recirculation circuit for ink-jet microsystems applications with fluids that contain a particle size of 40 nm to 10 μm. This analysis integrates multiple mathematical and experimental models, in regard to variables such as: viscosity change with temperature and solid volume fraction, sedimentation, surface tension and flow behavior. As a result, specific values of vacuum pressure for different drop-on-demand print heads with different ink-jet functional fluids, places of probable sedimentation and minimum pickup velocities to remove settled particles are given.

List of symbols

δ	Laminar sublayer thickness
η	Dynamic viscosity of the fluid
γ	Surface tension
κ_i	Coefficient of polynomial function $\eta(T)_{\text{IFF}-2}$
λ_i	Coefficient of polynomial function $\psi(\beta)$ where $0 \leq \beta \leq 1.2$
ν	Kinematic viscosity
ϕ	Solid volume fraction of the mixture
ψ	Correction factor Harkins and Brown
ρ_f	Fluid density
ρ_m	Mixture density
ρ_p	Particle density
κ_i	Coefficient of polynomial function $\eta(\phi)_{\text{IFF}-2}$
ϖ_i	Coefficient of polynomial function $\eta(\phi)_{\text{IFF}-1}$
ϑ_i	Coefficient of polynomial function $\psi(\beta)$ where $1.2 \leq \beta \leq 1.6$
ξ_i	Coefficient of polynomial function $\eta(T)_{\text{IFF}-1}$
C_D	Drag coefficient
D	Pipe diameter
d_p	Particle diameter
f	Friction factor due pipe flow
F_{st}	Force due surface tension
FA	Adhesion force on a particle
FB	Buoyant force on a particle
FD	Drag force on a particle
FF	Friction force on a particle
FL	Lifting force on a particle
FW	Gravity force on a particle
fs	Dry friction factor
g	Gravitational constant
h_p	Energy loss in pipes
k	Loss coefficient factor for accessories
P	Fluid pressure
r	Particle radius
r_n	Nozzles radius
Re	Reynolds number
T	Temperature
U	Pickup velocity
U_R	Uncertainty of a parameter R
V	Average fluid velocity
V_D	Drop volume
V_s	Settling velocity of a particle

✉ Manuel Cañas
mcanasa@eafit.edu.co

Ivan Arango
iarango@eafit.edu.co

[1] Universidad EAFIT, Carrera 49 No 7 Sur-50, Medellin, Colombia

Z	Height difference between points
B(1–2)	Pump 1 to Pump 2
BDG	Butyl diglycol
BST	Barium strontium titante
DG	Diethylene glycol
DOD	Drop-on-demand
E(1–4)	Elbow 1 to Elbow 4
F(1–5)	Fitting 1 to Fitting 5
FF	Functional Fluid
IFF	Ink-Jet Functional Fluid
P(1–10)	Pipe 1 to Pipe 10
PZT	Piezoelectric Actuator
T(1–3)	Tank 1 to Tank 3
V(1–2)	Valve 1 to Valve 2

1 Introduction

The advance of ink-jet printing technology has reached applications that allows to distinguish the uses between inks and functional fluids (FF). The first ones are used to give color while the FF are used to create and develop all kinds of entities. Ink-jet functional fluids (IFF) have been widely used in several applications such as: electronic devices (Friederich et al. 2015), microsystems (Kim et al. 2014), deposition of living cells (Tse et al. 2016), bioprinting (Binder et al. 2011) and 3D printing of ceramic components (Özkol 2013). The inclusion of nano and micro particulate material (pigments, silver particles, ceramic particles) conform a suspension which has to accomplish the rheological properties in relation to its application (Woo et al. 2013) and, at the same time, avoid the agglomeration to prevent damage or obstructions in the printing nozzles.

The inks and IFF have been deeply investigated from the chemical science point of view, contributing to controlling the physicochemical and rheological characteristics (Özkan et al. 2016), the generation of ecological inks (Robert 2015) and in the inclusion of some supplements that modify the properties of the fluid, such as surfactants which reduce surface tension (Soleimani-Gorgani et al. 2014) and dispersing agents to prevent the agglomeration of particles (Parsa et al. 2010). In hydraulic science, the recirculating fluids systems are made to supply fluid to the print head, forming a closed loop mechanical subsystem, allowing the constant movement of the functional fluid to prevent the agglomeration and sedimentation of particles and improve the print quality.

As a central part of ink-jet technology, print heads are extensively investigated. Drop-on-demand (DOD) print heads are commonly used in homes, offices and industry. Many DOD print heads have piezoelectric (PZT) actuators, which, when a voltage is applied, a charged droplet is ejected by the nozzles. Investigations about piezoelectric actuators have been taken from a mechanical perspective (Chang et al. 2016), electrical perspective (Kim et al. 2008) and it has reached the generation of new printing head designs (Maria et al. 2015; Sadeghian et al. 2014)

Sedimentation is a danger in print heads and recirculating systems; therefore, the understanding of this phenomena is necessary for an appropriate design of a recirculation system to avoid clogging in the device and print heads. Shields was the first person to study the incipient motion of sediment in a non-dimensional way (Shields 1936). Since then, several investigations about sedimentation have been registered (Gorrick and Rodríguez 2014; Wu et al. 2014). One of the approximations to treat sedimentation is on a flow conveying system with pick up velocity models to start the incipient motion of the settled particles in horizontal channels (Rabinovich and Kalman 2011).

The conservation and control of fluids properties must be taken into account in order for the recirculation system to function properly. Properties such as density and viscosity are affected by the presence of the micro and nano particles inside mixtures of the functional fluids (Liu et al. 2013). Several studies of changes in fluid viscosity as an effect of the inclusion of particles have been carried out (e.g., Einstein 1906; Batchelor 1977; Mendoza and Santamaria-Holek 2009; Dörr et al. 2013). In the case of ink-jet applications, the Krieger and Dougherty (1959) model is used because it better describes the non-colloidal systems. However, these models require experimental data to achieve accurate results, precluding the use of a purely theoretical model.

Another important property of IFF is surface tension, which performs a special role in drop formation and the printability, making imperative the supervising and regulation of this property. A large surface tension can make the ejection of the drop difficult, but, a small value would cause the involuntary release of the fluid. This property has been extensively studied by Harkins and Brown (1919). Further investigations have reached the generation of computational models of drop formation (Dadvand et al. 2011).

It is very common to find different challenges in the industry about the fluid functionality and quality, such as the electronics industry which seeks conductivity, resistivity and capacitance in new functional fluids to print sensors and electrical circuits (Kumashiro et al. 2009; Varela et al. 2011) or the ceramic industry, whose functional fluids have to withstand high temperatures without affecting its features and the printing quality (Güngör et al. 2016; Pan et al. 2015). In most cases, these challenges are studied from the chemical composition of functional fluids and their different properties.

Despite the existence of patents of recirculation circuit functional fluids, scientific literature has not registered studies or investigations about these circuits from the point of

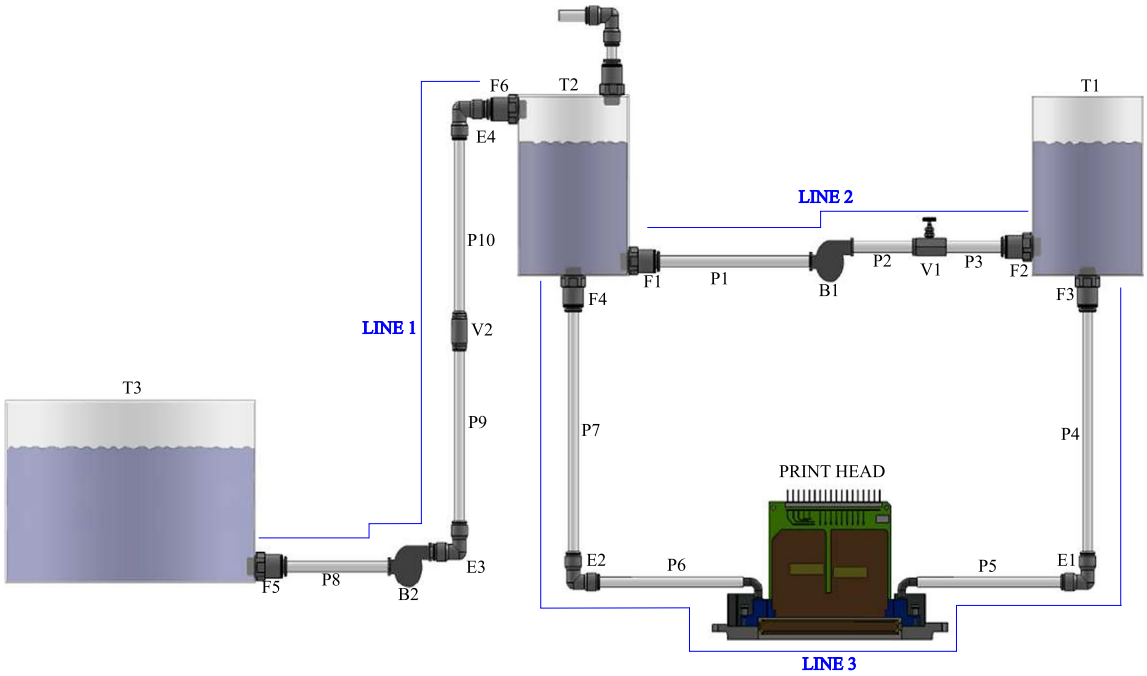

Fig. 1 Typical recirculation fluid system for ink-jet applications. The fluid is constantly moving to avoid agglomeration and sedimentation

view of physics law. This paper presents a dynamic analysis of a recirculation circuit for ink-jet microsystems applications with nano and micro fluids that contain a particle size of 40 nm to 10 μm with complete mathematical models including the sedimentation, surface tension phenomena, viscosity changes by the effect of temperature and solid volume fraction and change in density as a function of the volume phase.

2 Methodology

A typical fluid recirculation system of ink-jet technology is shown in Fig. 1. The system consists of three tanks, pipe line networks, pumps, valves and fittings. The IFF flows from tank 2 (T2) to tank 1 (T1) by the action of pump 1 (B1) across the needle valve (V1) and pipes 1 (P1), 2 (P2) and 3 (P3). The fluid returns to T2 going through the print head by effect of the static pressure difference between T1 and T2. Slight vacuum pressure is established in T2 to prevent leaking from the print head and regulate the meniscus pressure presented in the print head nozzles. Tanks 1 and 3 are exposed to atmospheric pressure. When the volume of fluid in T1 and T2 are low, pump 2 (B2) is activated and initiates the flow from reservoir tank (T3) to T2. A unidirectional valve (V2) is placed before T2 to prevent the flow from T2 to T3. For clarity, the pipe line formed by pipes 8 (P8), 9 (P9) and 10 (P10), B2, V2, elbows 3 (E3) and 4 (E4), fitting 5 (F5) and 6 (F6) is called line 1. Line 2 consists of fittings 1 (F1) and 2 (F2), P1, P2 and P3, B1 and V1 and line 3 are formed by pipes 4 (P4), 5 (P5), 6 (P6) and 7 (P7), fittings 3 (F3) and 4 (F4), elbows 1 (E1) and 2 (E2) and the print head.

The dynamical model of the recirculation system includes the estimation of the pressure in any point of the lines, flow rate, variation of viscosity by effect of temperature and inclusion of spherical particles, and sedimentation in the most critical places of the system. The sections below shown the mathematical models and the equations used in the numerical method employed in the dynamical simulation. The value of friction factor (K) to compute the pressure losses by effect of the elbow is 1.1, 0.8 for fittings and 4 for valves. The friction factor (f) due to the flow in pipes is calculated by the Colebrook–White equation for turbulent regimen flow; laminar flow is found by 64/Re. The typical internal diameter of the pipes is 2.5 mm, the length of P1 is 100 mm; P2 and P3 are 30 mm; P4 and P7 are 100 mm; P5, P6 and P8 are 20 mm; P9 and P10 are 35mm; the roughness of the material is 0.00015 mm. The power of the pumps is 3W with a maximum flow rate of 155 ml/min, the curves are obtained experimentally and then integrated to the model by an interpolate curve. In the dynamical analysis, two ink-jet functional fluids are used based on the results of Friederich et al. (2013) and Tajamid and Guenther (2010). The properties of the IFF are listed in Table 1. The density and viscosity of the two suspensions are the initial values with a temperature of 20 ° C and with the specified volume fraction. Density of barium strontium titanate (BST) is 5840 kg/m^3 (2015) and 10500 kg/m^3 for silver.

Table 1 Ink-jet functional fluids properties based on the works of Friederich et al. (2013) and Tajamid and Guenther (2010)

Parameter	IFF-1	IFF-2
Solids content material	BST	Ag
Solids size (nm)	270	40
Solid volume fraction (%)	4.91	0.5
Solvent	BDG	DG
Suspension density (kg/m^3)	1180	1166
Surface tension (mN/m)	30	33
Suspension viscosity (mPa s)	8.4	22.25

Both IFF are used in the microsystems manufacturing

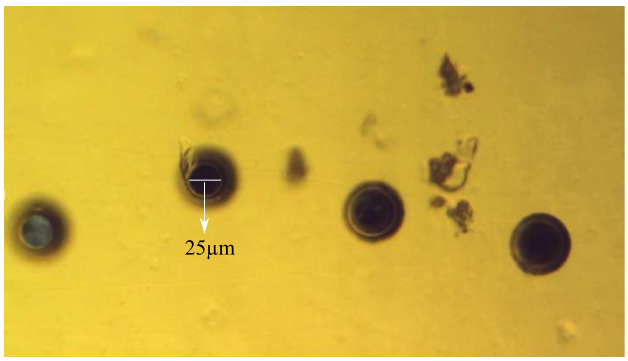

Fig. 2 Nozzle diameter of Print Head 1 (25 µm)

The density of Butyl Diglycol (BDG) is 956 and 1120 kg/m^3 for diethylene glycol (DG), the viscosity of butyl and diethylene is considered as 5.9 and 16.2 mPa s, respectively. The density and viscosity of Toluene are 867 kg/m^3 and 0.59 mPa s. Figure 2 shows the nozzle diameter of a print head of 5–7 picoliters.

The dynamical analysis is focused on three different print heads in shear mode described in Table 2. The width of the piezoelectric channel is 2:1 or 2.5:1 in respect to the nozzle diameter. The roughness of the channel is assumed as 0.0015 mm. The depth of the piezoelectric is four or five times the width; the thickness of the piezoelectric is 1.25:1 in respect to the width of the channel, and even in some print heads it can be 1:1. The diameter of the main ink conduct inside the print heads is assumed as 1.7 mm. The main duct provide fluid to the piezoelectric actuators who are located to the longitudinal sides of the main duct. The flow through the piezoelectric actuators were estimated by the Hardy Cross method.

2.1 Uncertainty analysis

The uncertainty of the most important parameters are described in Table 3. The kinematic viscosity can be measured with VS-2500 viscosity sensor, flow rate with

Table 2 Geometrical properties of the print heads

Parameters	Print Head 1	Print Head 2	Print Head 3
Drop volume (pl)	5–7	14–16	83–86
Nozzle diameter (µm)	25	30	50
Main conduct length (mm)	65	70	75
PZT Width channel (µm)	85	75	100
PZT thickness (µm)	85	94	125
PZT depth channel (µm)	340	469	450
PZT length channel (µm)	1000	1500	2000

The Nikon Eclipse Ci-l © microscope is used to measure the nozzle diameter of three print heads. The other properties are taken from proportions found in the literature (Wallace et al. 1998; Wu and Lai 2009) and experimental measurements

FLR1009ST, the pressure with a SDP610 sensor, the surface tension with a tensiometer T100 and the density with L-Dens 312 OEM. The uncertainty of this analysis were estimated by the Schultz and Cole method (1979), represented in Eq. (1).

$$U_R = \left[\sum_{i=1}^{n}\left(\frac{\partial R}{\partial V_i}U_{V_i}\right)^2\right]^{1/2} \tag{1}$$

Where U_R is absolute the uncertainty of a parameter R which is a function of some measured parameters V_i; n is the number of parameters and U_{V_i} is the absolute uncertainty of indepenpedent parameters. At the maximum flow rate, the velocities were estimated to have less than ±3% error, and as a consequence, the expected Reynolds error is about ±4%. The maximum error for the Eq. (2) is about ±4% and for the pick up velocity about ±5%. For Eq. (14) the maximum error is ±3%.

3 Mathematical model

3.1 Flow, pressure and sedimentation in pipe lines

Pressure and velocity of the FF in any point of the recirculating system is calculated by:

$$\frac{P_1}{\rho_f g}+\frac{V_1^2}{2g}+Z_1=\frac{P_2}{\rho_f g}+\frac{V_2^2}{2g}+Z_2+\sum h_p \tag{2}$$

In which P is the pressure in a selected point; ρ_s is the density of the fluid, g is the acceleration of gravity, V is the average velocity at the point; Z is the height difference in respect to a reference system; h_p is the energy loss due to frictional accessories or tubes.

Sedimentation can occur in tanks and pipes and, to prevent this situation, dispersants are added to the fluid which generate repulsive forces between particles. However, when the fluid is static or the velocity of the fluid is too

Table 3 Absolute uncertainties of the basic parameters of the mathematical model

Parameter	Absolute uncertainty
Pipe length (mm)	±0.5
Pipe diameter (mm)	±0.05
Kinematic viscosity (cSt)	±0.1
Flow rate (ml/min)	±5
Pressure (Pa)	±0.5
Density (gr/m^3)	±0.001
Surface tension (mN/m)	±0.1

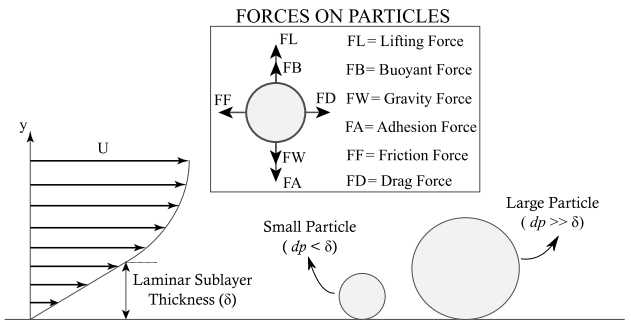

Fig. 3 Scheme of a settled particle. A free body diagram is provided for a insulated particle

low, the gravity force exceeds the repulsive forces and, as a consequence, the sedimentation and agglomeration of the particles occur. The falling settling velocity of an insulate particle in concentrated suspension is a modification of the Stokes equation and is given by Eq. (3).

$$V_s = \frac{2(\rho_p - \rho_f)gr^2}{9\eta}(1-\phi)^{5\pm0.25} \tag{3}$$

where V_s is the sedimentation velocity, r is the particle radius assuming spherical particles, ρ_p is the density of the particle, η is the dynamic viscosity of the fluid, ϕ is the phase volume. The exponent is 4.75 when the radius of the particle is greater than 1 μm and 5.25 for submicron particles. This expression is useful in finding the time that it takes a particle to travel a certain distance, and as a consequence, the time that the recirculation fluid system can turn off.

The pickup velocity is an important variable in conveying systems. To ensure the proper functioning of the recirculating system, the velocity of the fluid must be maintained at the minimum pickup velocity. Assuming a settled particle at the bottom of the channel as Fig. 3 shows, the pickup velocity for large particles can be calculated with Eq. (4) proposed by Cabrejos and Klinzing (1992). Equation (5) proposed by Hayden et al. (2003) can be used to find the minimum pick up velocity for small particles.

As Cabrejos and Klinzing (1992) expose, a particle is considered "large" when the diameter of the particle is greater than the thickness of the laminar sublayer of the fluid ($d_p \gg \delta$). When the diameter of the particle lies within the thickness of the laminar sublayer ($d_p < \delta$), it is considered as "small".

$$U = \left[1 - \left(\frac{d_p}{D}\right)^{1.5}\right]\sqrt{\frac{4}{3}\frac{f_s g d_p}{C_D}\left(\frac{\rho_p - \rho_f}{\rho_f}\right)} \tag{4}$$

$$U = \frac{2.62\nu^{\frac{13}{21}}D^{\frac{3}{21}}}{\eta^{\frac{8}{21}}}\left(\frac{\pi}{6}g(\rho_p - \rho_f) + \frac{1.302e-6}{d_p^2}\right)^{\frac{8}{21}} \tag{5}$$

where d_p is the diameter of the particle, D is the diameter of the pipe, f_s is a friction factor equal to the tangent of the angle in which a particle begins to slide, ν is the kinematic viscosity of the fluid and C_D is the drag coefficient.

3.2 Viscosity and density

The viscosity and density significantly affect variables such as pressure and velocity of the fluid. The change of these properties can be produced by several factors such as temperature change and solid content. The tanks and some print heads have internal resistances to heat the functional fluid making the operational temperature of IFF change between 20 and 60 °C. As a consequence, the functional fluid changes the temperature in time to achieve an operational fluid temperature. In the industry, there are all kinds of IFF with different solid volume phases, making the analysis of change of viscosity with different amounts of solid volume fractions imperative.

The experimental curves of the viscosity changes with temperature changes and solid volume fractions are obtained from the results of Friederich et al. (2013) and Tajamid and Guenther (2010). The polynomial equations of interpolated curves of the IFF-1 and IFF-2 are shown in Eqs. (6)–(9). Table 4 shows the constants values of the Eqs. (6)–(9), (12) and (13).

$$\eta(T)_{\mathrm{IFF}-1} = \sum_{i=0}^{7} T^i \xi_i \quad 20\,^\circ C \leqslant T \leqslant 60\,^\circ C \tag{6}$$

$$\eta(T)_{\mathrm{IFF}-2} = \sum_{i=0}^{7} T^i \varphi_i \quad 15\,^\circ C \leqslant T \leqslant 35^\circ C \tag{7}$$

$$\eta(\phi)_{\mathrm{IFF}-1} = \sum_{i=0}^{7} \phi^i \varpi_i \quad 5\% \leqslant \phi \leqslant 32\% \tag{8}$$

$$\eta(\phi)_{\mathrm{IFF}-2} = \sum_{i=0}^{7} \phi^i \kappa_i \quad 0\% \leqslant \phi \leqslant 4.37\% \tag{9}$$

Table 4 Constants values for interpolated Eqs. (6)–(9), (12) and (13)

i	ξ_i	φ_i	ϖ_i	κ_i	λ_i	ϑ_i
0	37.749	285.475	−42.742	21.34	1	36.866
1	−0.9849	−37.554	1644.331	−782.8	−0.9121	103.995
2	0.01662	2.165	−16951.8	221924	−2.109	−107.211
3	−0.000293	−0.05667	52186.9	-9.65×10^{6}	13.38	48.799
4	2.671×10^{-6}	0.000554	0	1.19×10^{8}	−27.26	−8.303
5	0	0	0	0	27.53	0
6	0	0	0	0	−13.58	0
7	0	0	0	0	2.593	0

Table 5 Maximum flow rates (ml/min) at line 3

	Maximum flow rate (ml/min)		
FF	Print Head 1	Print Head 2	Print Head 3
IFF-1	33	31	30
IFF-2	29	28	27

These flow rates occur when the height is 115 and 0 mm in T1 and T2, respectively

where T is the temperature of the fluid in ℃ and ϕ is the solid volume fraction Eqs. (6), (7), (8) and (9) are valid in the specified ranges. The density of the suspension is also affected by the increase of the solid content. To calculate the density of the suspension, Eq. (10) is used where ρ_m is the density of the mixture and ϕ is the solid volume fraction (Poletto and Joseph 1995).

$$\rho_m = \rho_f(1-\phi) + \rho_p\phi \tag{10}$$

3.3 Surface tension

In the jetting mode, the pressure induced by the PZT actuator on the print head has to exceed the viscosity and capillarity pressure produced by the surface tension to expulse the drop. In non-jetting mode, the surface tension has to be equal or greater than the pressure of the column of the fluid above the nozzle. The force on the drop due to the surface tension has been calculated with the Eq. (11) (Lee et al. 2012).

$$F_{\mathrm{st}} = 2r_n\gamma\psi\pi \tag{11}$$

where F_{st} is the force of the surface tension, r_n is the radius of the nozzle, γ is the surface tension of the fluid and ψ is the correction factor of Harkins and Brown (1919), which can be calculated by Eq. (12) proposed by Lee et al. (2008) or Eq. (13) suggested by Pu and Chen (2001).

$$\psi(\beta) = \sum_{i=0}^{7}\beta^i\lambda_i \tag{12}$$

$$\psi(\beta) = \sum_{i=0}^{7}\beta^i\vartheta_i \tag{13}$$

where $\beta = r_n/(V_{\mathrm{D}}^{1/3})$ and V_{D} are the volume of the drop. Equation (12) is only applicable when $0 \le \beta \le 1.2$. Meanwhile, Eq. (13) is applicable when $1.2 \le \beta \le 1.6$.

The force of the surface tension divided by the area of the nozzle gives the pressure of the surface tension shown in Eq. (14), according to the Laplace equation with the Harkins and Brown (1919) correction factor included. It is assumed that the drops will be spherical and will have the same diameter that the nozzles print head at the lower jetting frequency.

$$\Delta P = \frac{2\gamma\psi}{r_n} \tag{14}$$

4 Results and discussion

4.1 Flow and settling in pipe lines and tanks

In order to analyze the effects of the height fluid in tanks on the flow rate, the results of this section will be presented without taking the vacuum pressure in T2 into account. Since the powers of B1 and B2 are the same, the maximum flow rate occurs in P1 and E3 with a value of 153 ml/min with IFF-1 at 20 ℃. When the fluid is replaced by IFF-2, the flow rate decrease to a 148 ml/min. The reason for the decrease in the flow is a consequence of a higher viscosity of IFF-2. As a result, the maximum number Reynolds is about 182 and consequently the flow is completely laminar. Then, Poiseuille's law is applicable in all pipe lines.

The flow rate at line 3 is governed by the height fluid of tanks (without pumps), and as a result the lowest flow rate of all lines is presented in this line with a maximum flow rate of 33 ml/min showed in Table 5.

As Eq. (2) expose, the pressure and velocity of a fluid are high correlated, so that the pressure change caused by the different print heads affect the fluid velocity at line 3. Consequently, there is difference in flow rates by reason of different print heads. Table 5 shows that the maximum flow rate at line 3 is always with Print Head 1, being that the pressure drop in this print head is lower than the Print Heads 2 and 3. On the other hand, the heights fluids in the tanks affect the pressure at the line 3, so if the difference

Table 6 Settling time of powders of other IFF used in microsystems manufacturing

Solvent	Powder	Particle size diameter (μm)	Density powder (kg/m^3)	Solid volume fraction (%)	Time (h)
BDG	TiO_2	0.08	4230	10	25
BDG	Co_3O_4	5	6110	25	0.009
Toluene	Au	1	19,300	25	0.007

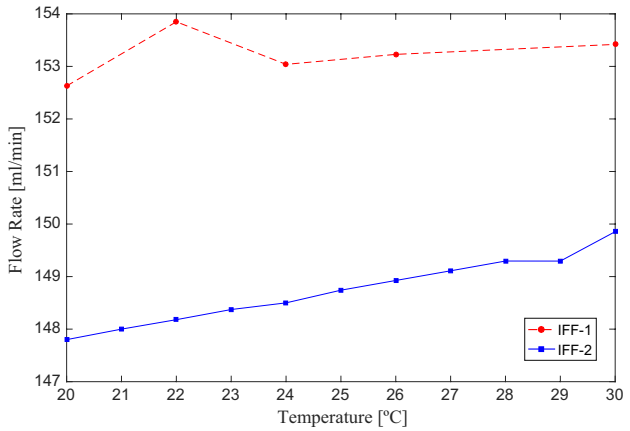

Fig. 4 Flow rate (ml/min) vs temperature (°C). Solid volume fraction and viscosity are constants to this figure (see Table 1)

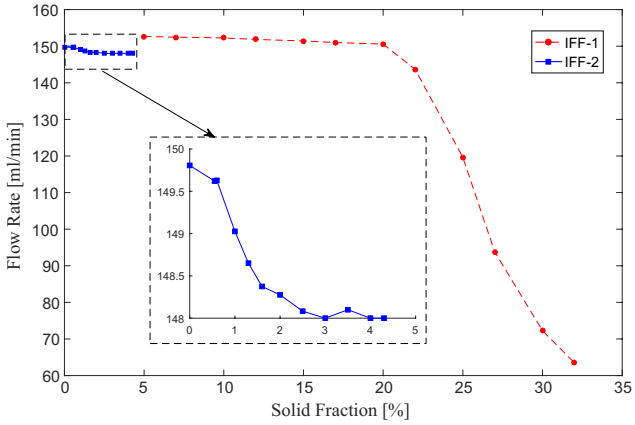

Fig. 5 Flow rate (ml/min) vs solid volume fraction (%). The change of the flow rate with the variation of the solid volume fraction at 20 °C at *lines* 1 and 2

between the heights fluids of the two tanks diminishes, so will the flow at line 3. In order to keep a constant flow through line 3, a constant height difference of the fluid in the tanks is necessary.

The change of the flow rate as a function of temperature at lines 1 and 2 is shown in Fig. 4. This variation is plotted in the range of 20–30 °C; however, the total range of the temperatures is greater as displayed in Eqs. (6) and (7).

As the temperature of the ink-jet functional fluid increases, the viscosities goes down. As a result, the pressure losses decreases and there is an increase in the flow rate. The flow boost an overall of 2 ml/min with IFF-1 at lines 1 and 2, while the total variation with IFF-2 is about 4 ml/min at the same lines. The same proportions occur with the flow through line 3. This results takes into account the solid volume fraction of each IFF.

The flow rate at lines 1 and 2 has a decrease with IFF-1 close to 88 ml/min when the solid volume fraction is about 32% (see Fig. 5). This abrupt decrease in the flow rate is a result of two factors: the sharp increase of the relative viscosity when the solid concentration is greater than 30% as Özkol (2013) and Lee et al. (2005) exposed and the increase of density. For the flow rate with IFF-2, the overall variation is about 1.5 ml/min by reason of the low concentration of solid. For line 3, the dynamic analysis shows no immediate flow with IFF-1 with 32% of solid content because the gravity is not enough to move the fluid at that

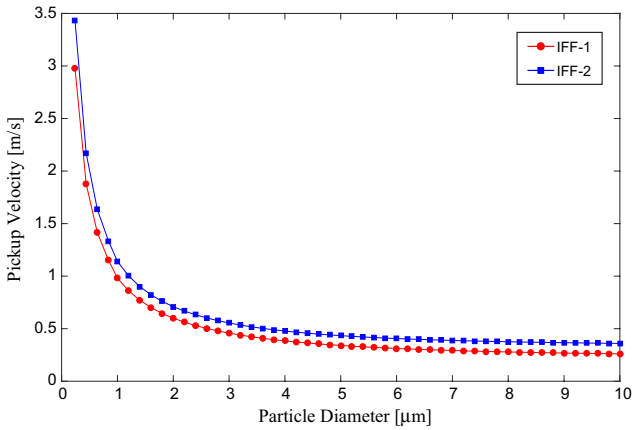

Fig. 6 Pickup velocity (m/s) vs particle diameter (μm)

solid concentration. With the IFF-2 there is an overall decrease of 1.3 ml/min at line 3.

The lower Reynolds in the pipes shows that the particles lie in the laminar sublayer, so Eq. (5) can be employed to estimate the minimum fluid velocity through the pipes. Figure 6 shows the minimum pickup velocity of the two IFF as a function of particle diameter.

The minimum velocities to move the settled particles of the IFF-1 ($d_p = 270$ nm) are about 2.7 and 7.7 m/s for the particles of IFF-2 ($d_p = 40$ nm). Van der Waals forces

increase as the particle diameter decrease and consequently the required fluid velocity to move a settled particle increase as the particle diameter decrease. It should be noted that the model used to compute this velocity has not taken the full range of the Safman model for a lifting force as Rabinovich and Kalman (Rabinovich and Kalman 2011) exposed; therefore, the results are just a first approximation.

The lowest flow rates are at line 3 and, consequently, the highest probabilities of sedimentation. The pickup velocity to move a silver particle of a diameter of 5 μm with the solvent of the IFF-2 is about 0.43 m/s. This implies a flow of 128 ml/min and a difference fluid height of more than 500 mm in tanks. To increase the velocity through the pipes, a pump and filter between T2 and the print head should be implemented.

With the purpose of knowing the settling time of a particle in the tank when the fluid is static, a distance of 0.1 mm between the bottom of the sphere and the bottom of the tank is assumed. The estimation of the time is about 1 h for IFF-1 and 56 hours for the particles of IFF-2. Table 6 shows other usual IFF with ceramic (TiO_2, Co_3O_4) (Zhang et al. 2008) and conductive (Au) powders and its respective time with the same distance.

As the results suggest, the ink-jet recirculating system should never be turned off, especially when the diameter of the particles are higher than 2 μm. Equation (3) shows that as long as the solid volume fraction increases, the settling velocity will be lower as an effect of the increase of viscosity. These results can be useful as a first approximation due to the fact that the Stokes law is not accurate at nano-scale and other interactions appear such as Van der Waals forces. A mechanical solution to this issue is assembly propellers inside the tank working constantly avoiding the sedimentation of the particles at the bottom of the tank.

4.2 Vacuum pressure

The force produced by the fluid column above of the print head over the nozzles, must be into account to avoid the leaking of the fluid from the nozzle plate. If the force of the fluid column is higher than the surface tension force, then, the leak will occur immediately and profusely. Using Eq. (11) it can be estimated the maximum height of two IFF with the different print heads with other common fluids used in ink-jet technology (see Table 7). The density of aqueous functional fluid and oil-based FF is assumed as 1770 kg/m^3 and 1088 kg/m^3, respectively. The surface tension of oil-based FF is 30 mN/m (Hutchings and Martin 2013) and aqueous FF as 46 mN/m (Cappi et al. 2011).

The data of Table 7 indicates that the recirculation fluid system has to be close to the print head in order to avoid print quality imperfections. These results concur with many industrial applications where the recirculation system is immediately above the print head. To place a recirculation system at a large distance, the vacuum pressure should balance the excess liquid column.

Even the force of the column of fluid above the nozzle is lower than the force of the surface tension, the wetting of the nozzle plate and later the leaking of the FF can occur by several reasons: Overfill the nozzles, Marangoni flows, defects of the nozzle plate, among others (Wijshoff 2008). This leaking can occur as much as jetting mode and non-jetting mode, generating the need of setting a vacuum pressure. The theoretical vacuum pressure needed to avoid the

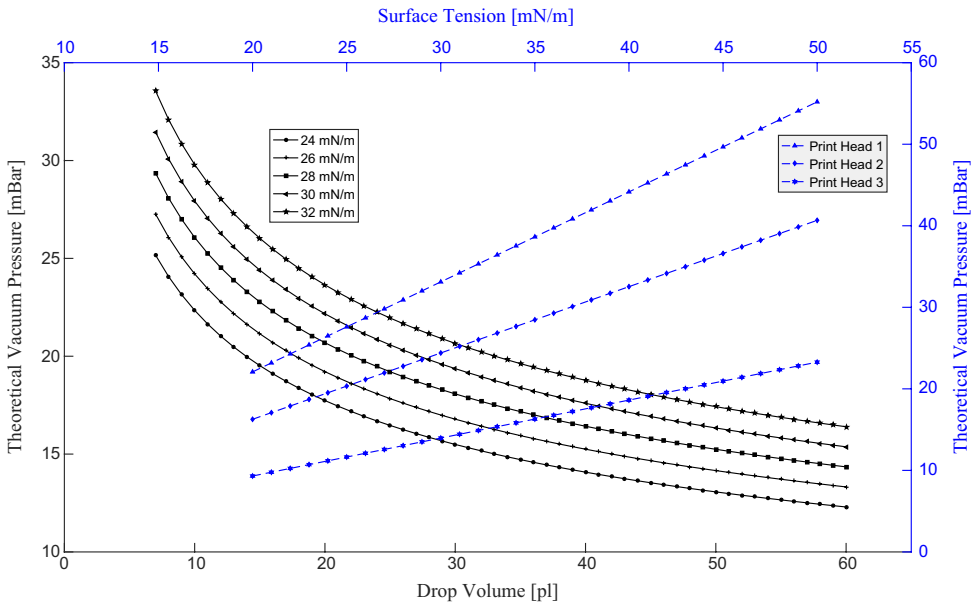

Fig. 7 Theoretical vacuum pressure (mBar) vs [drop volume (pl) and surface tension (mN/m)]. *Blue* plots (and scale) allows find a theoretical vacuum pressure given the surface tension of the FF for different print heads. *Black* plots allows obtain the vacuum pressure given the drop volume for different values of surface tension

Table 7 Maximum column height fluid

FF	Maximum column fluid height (m)		
	Print Head 1	Print Head 2	Print Head 3
IFF-1	0.218	0.186	0.113
IFF-2	0.282	0.241	0.146
Aqueous FF	0.259	0.221	0.134
Oil-based FF	0.274	0.234	0.142

formation of a drop with the same diameter as the nozzle print head is shown in Fig. 7. Over the full range of the graph, the correction factor (ψ) has a constant value of 0.622. Then, the vacuum pressure varies by reason of two parameters: Surface tension and nozzle radius. The pressure required to form a drop is smaller as the surface tension of the fluid decreases and the diameter of the print head nozzles increases. When a drop is formed and the wetting of the nozzle plate occurs the vacuum pressure is established given the surface tension and the print head nozzle diameter. This is a preventive and exploratory analysis, since it is assumed that requires a vacuum pressure equal to the pressure necessary to form the drop to avoid the formation of it.

The theoretical results have not taken into account the defects of the nozzle plate, the gradients of the surface tension and surfactants at the border of the nozzle, making the vacuum pressure to be higher or lower than the results; however, these results agree with the vacuum pressures established in the commercial recirculating fluid systems.

5 Conclusions

An ink-jet recirculation system was analyzed with a theoretical-practical complete model. The flow rate in recirculation ink systems can be affected by several variables such as: temperature change and solid concentration. The most significant variable that affects the flow rate is the solid volume fraction of the different IFF.

Minimum pickup velocity cannot be easily calculated due to the different variables involved. The theoretical pickup velocity can be easily achieved for particle diameter greater than 5 μm. The use of a pump and filters between tank 1 and the print head is necessary. The recirculation functional fluid system should always be working to avoid sedimentation in tanks and immediately above the print head. As a recommendation, the use of valves before and after the print head facilitates the maintenance of the system.

The values of vacuum pressure are given to different print heads and values of surface tension. A simple model is given to the use of industrial applications. The results has not been validated formally in the literature, but the selected mathematical models are useful and are consistent with industrial and experimental observations.

References

Batchelor G (1977) The effect of brownian-motion in bulk stress in a suspensions of spherical particles. J Fluid Mech 87(1):97–117. doi:10.1017/S0022112077001062

Binder K, Allen AJ W, Atala A (2011) Drop-on-demand inkjet bioprinting: a primer. Gene Ther Regul 6(01):33–49. doi:10.1142/S1568558611000258

Cabrejos F, Klinzing G (1992) Incipient motion of solid particles in horizontal pneumatic conveying. Powder Technol 72(1):51–61. doi:10.1016/S0032-5910(92)85021-M

Cappi B, Ebert J, Telles R (2011) Rheological properties of aqueous si3n4 and mosi2 suspensions tailor-made for direct inkjet printing. J Am Ceram Soc 94(1):218–293. doi:10.1111/j.1551-2916.2010.04052.x

Chang J, Liu Y, Huang B (2016) Steady state response analysis of a tubular piezoelectric print head. Sensors 16(1):81. doi:10.3390/s16010081

Ćirković J, Vojisavljevi-ć K, Nikoli-ć N, Vuli-ć P, Brankovi-ć Z, Sre-ćkovi-ć T, Brankovi-ć G (2015) Dielectric and ferroelectric properties of BST ceramics obtained by a hydrothermally assisted complex polymerization method. Ceram Int 41(9, Part A):11,306–11,313. doi:10.1016/j.ceramint.2015.05.088

Dadvand A, Shervani-Tabar M, Khoo B (2011) A note on spark bubble drop-on-demand droplet generation: simulation and experiment. Int J Adv Manuf Tech 56(1–4):245–259. doi:10.1007/s00170-011-3165-1

Dörr A, Sadiki A, Mehdizadeh A (2013) A discrete model for the apparent viscosity of polydisperse suspensions including maximum packing fraction. J Rheol 57(3):743–765. doi:10.1122/1.4795746 (**1978-present**)

Einstein A (1906) A new determination of the molecular dimensions. Ann Phys 19(4):289–306

Friederich A, Binder J, Bauer W (2013) Rheological control of the coffee stain effect for inkjet printing of ceramics. J Am Ceram Soc 96(7):2093–2099. doi:10.1111/jace.12385

Friederich A, Kohler C, Nikfalazar M, Wiens A, Jakoby R, Bauer W, Binder J (2015) Inkjet-printed metal-insulator-metal capacitors for tunable microwave applications. Int J Appl Ceram Technol 12(S1). doi:10.1111/ijac.12362

Güngör G, Kara A, Gardini D, Blosi M, Dondi M, Zanelli C (2016) Ink-jet printability of aqueous ceramic inks for digital decoration of ceramic tiles. Dyes Pigm 127:148–154. doi:10.1016/j.dyepig.2015.12.018

Gorrick S, Rodríguez J (2014) Scaling of sediment dynamics in a laboratory model of a sand-bed stream. J Hydro Environ Res 8(2):77–87. doi:10.1016/j.jher.2013.12.001

Harkins W, Brown F (1919) The determination of surface tension (free surface energy), and the weight of falling drops: The surface tension of water and benzene by the capillary height method. J Am Chem Soc 41(4):499–524. doi:10.1021/ja01461a003

Hayden KS, Park K, Curtis JS (2003) Effect of particle characteristics on particle pickup velocity. Powder Technol 131(1):7–14. doi:10.1016/S0032-5910(02)00135-3

Hutchings I, Martin G (2013) Inkjet technology for digital fabrication. Wiley, Chichester

Kim J, Grisso B, Kim J, Ha D, Inman D (2008) Electrical modeling of piezoelectric ceramics for analysis and evaluation of sensory

systems. En Sensors Applications Symposium, 2008 SAS 2008 IEEE pp 122–127

Kim Y, Ren X, Ki J, Noh H (2014) Direct inkjet printing of micro-scale silver electrodes on polydimethylsiloxane (pdms) microchip. J Micromech Microeng 24(11):115,010, 10.1088/0960-1317/24/11/115010

Krieger I, Dougherty T (1959) A mechanism for non-newtonian flow in suspensions of rigid spheres. Trans Soc Rheol 137(3):137–152. doi:10.1122/1.548848

Kumashiro Y, Nakako H, Inada M, Yamamoto K, Izumi A, Ishihara M (2009) Novel materials for electronic device fabrication using ink-jet printing technology. Appl Surf Sci 256(4):1019–1022. doi:10.1016/j.apsusc.2009.05.134

Lee B, Ravindra P, Chang E (2008) A critical review: surface and interfacial tension measurement by the drop weight method. Chem Eng Comm 195(8):889–924. doi:10.1080/00986440801905056

Lee H, Chou K, Huang K (2005) Inkjet printing of nano-sized silver colloids. Nanotechnology 16(10):2436–2441. doi:10.1088/0957-4484/16/10/074

Lee S, Nguyen X, Ko H (2012) Study on droplet formation with surface tension for electrohydrodynamic inkjet nozzle. J Mech Sci Technol 26(5):1403–1408. doi:10.1007/s12206-012-0301-y

Liu Y, Tsai M, Pai Y, Hwang W (2013) Control of droplet formation by operating waveform for inks with various viscosities in piezoelectric inkjet printing. Applied Physics A 111(2):509–516. doi:10.1007/s00339-013-7569-7

Maria CD, Ferrari L, Montemurro F, Vozzi F, Guerrazzi I, Bolan T, Vozzi G (2015) Design and validation of an open-hardware print-head for bioprinting application. Procedia Engineering 110:98–105. doi:10.1016/j.proeng.2015.07.015

Mendoza C, Santamaria-Holek I (2009) The rheology of hard sphere suspensions at arbitrary volume fractions: An improved differential viscosity model. J Chem Phys 130(4):044,904. doi:10.1063/1.3063120

Özkol E (2013) Rheological characterization of aqueous 3ytzp inks optimized for direct thermal ink jet printing of ceramic components. J Am Ceram Soc 96(4):1124–1130. doi:10.1111/j.1551-2916.2010.04052.x

Özkan M, Dimic-Misic K, Karakoc A, Hashmi S, Lund P, Maloney T, Paltakari J (2016) Rheological characterization of liquid electrolytes for drop-on-demand inkjet printing. Org Electron 38:307–315. doi:10.1016/j.orgel.2016.09.001

Pan Z, Wang Y, Huang H, Ling Z, Dai Y, Ke S (2015) Recent development on preparation of ceramic inks in ink-jet printing. Ceram Int 41(10, Part A):12,515–12,528. doi:10.1016/j.ceramint.2015.06.124

Parsa S, Gupta M, Loizeau F, Cheung K (2010) Effects of surfactant and gentle agitation on inkjet dispensing of living cells. Biofabrication 2(2):025. doi:10.1016/j.jeurceramsoc.2014.04.030

Poletto M, Joseph D (1995) Effective density and viscosity of a suspension. J Rheol 39(2):323–343. doi:10.1122/1.550692

Pu B, Chen D (2001) A study of the measurement of surface and interfacial tension by the maximum liquid drop volume method. J Colloid Interface Sci 235(2):265–272. doi:10.1006/jcis.2000.7385

Rabinovich E, Kalman H (2011) Threshold velocities of particle-fluid flows in horizontal pipes and ducts: literature review. Rev Chem Eng 27(5–7):215–239. doi:10.1515/REVCE.2011.011

Robert T (2015) Green ink in all colors-printing ink from renewable resources. Prog Org Coat 78:287–292. doi:10.1016/j.porgcoat.2014.08.007

Sadeghian H, Hojjat Y, Ghosi M, Sheykholeslami M (2014) An approach to design and fabrication of a piezo-actuated micro-droplet generator. Int J Manuf Technol 70(5–8):1091–1099. doi:10.1007/s00170-013-5371-5

Schultz R, Cole R (1979) Uncertainty analysis in boiling nucleation. AIChE symposium series 75:32–38

Shields A (1936) Application of similarity principles and turbulence research to bed-load movement. California Institute of Technology (**report 167**)

Soleimani-Gorgani A, Bakhshandeh E, Najafi F (2014) Effect of dispersant agents on morphology and optical-electrical properties of nano indium tin oxide ink-jet ink. J Eur Ceram Soc 34(12):2959–2966. doi:10.1016/j.jeurceramsoc.2014.04.030

Tajamid E, Guenther B (2010) Rheological and sedimentation behaviour of nanosilver colloids for inkjet printing. Int J Nanomanuf 5(3–4):383–392. doi:10.1504/IJNM.2010.033881

Tse C, Whiteley R, Yu T, Stringer J, MacNeil S, Haycock J, Smith, Patrick J (2016) Inkjet printing Schwann cells and neuronal analogue ng108-15 cells. Biofabrication 8(1):015,017. doi:10.1088/1758-5090/8/1/015017

Varela F, Armendáriz E, Wolluschek C (2011) Inkjet printed electronics: The wet on wet approach. Chem Eng Process 50(5–6):589–591. doi:10.1016/j.cep.2011.02.001

Wallace D, Trost H, Eichenlaub U (1998) Multi-fluid ink-jet array for manufacturing of chip-based microarray systems. In: Proc 2nd Int Conf Microreaction Technology

Wijshoff H (2008) Structure-and fluid-dynamics in piezo inkjet printheads. University of Twente, Enschede

Woo K, Jang D, Kim Y, Moon J (2013) Relationship between printability and rheological behavior of ink-jet conductive inks. Ceram Int 39(6):7015–7021. doi:10.1016/j.ceramint.2013.02.039

Wu Y, Lai W (2009) The simulation of the piezoelectric print head. Mod Phys Lett B 23(3):441–444. doi:10.1142/S0217984909018606

Wu Y, Xu H, Xu D, Bai Y (2014) Incipient velocity of non-uniform sediment in sloping river bends. Trans Tianjin Univ 20:163–167. doi:10.1007/s12209-014-2192-z

Zhang Y, Yang S, Chen L, Evans J (2008) Shape changes during the drying of droplets of suspensions. Langmuir 24(8):3752–3758. doi:10.1021/la703484w